INTERNATIONAL JOURNAL OF
NUMERICAL ANALYSIS AND MODELING
Volume 17, Number 3, Pages 434–456

AN ADAPTIVE VISCOSITY E–SCHEME FOR DEGENERATE CONSERVATION AND BALANCE LAWS

EBISE ADUGNA ABDI AND HANS JOACHIM SCHROLL

Abstract. An adaptive E–scheme for degenerate, viscous balance laws is presented. Taking into account natural diffusion, numerical viscosity is locally reduced to a minimum. Numerical experiments demonstrate the improved accuracy of the adaptive scheme. Explicit and implicit three–point E–schemes are monotone, TVD and nonlinearly stable. A high–resolution version of the adaptive E–scheme is derived and tested in experiments. The latter is not necessarily monotone, but TVD.

Key words. Balance law, E–scheme, monotone, degenerate viscosity.

1. Introduction

For scalar conservation laws $u_t + f(u)_x = 0$ the entropy solution may be constructed as the vanishing viscosity weak solution to the viscous conservation law $u_t + f(u)_x = du_{xx}$. Numerical methods for hyperbolic conservation laws appeal to that principle by using artificial, vanishing viscosity. For example, the classical Lax–Friedrichs scheme applies the numerical viscosity $d = \epsilon\Delta x$ where $\epsilon = 0.5\Delta x/\Delta t$. By the CFL–condition ϵ is bounded from below $2\epsilon \geq \|f'\|_\infty$. In agreement with the concept: sufficient diffusion grants stability, Tadmor [25] showed that any scheme containing more numerical viscosity than Godunov's scheme is entropy–stable. Moreover, it is exactly the class of E–schemes [21] that have no less numerical viscosity than that of Godunov.

In this paper we present an adaptive viscosity E–scheme for degenerate, viscous conservation laws

$$u_t + f(u)_x = (d(u,x)u_x)_x \quad , \quad d(u,x) \geq 0 \tag{1}$$

making use of the given "natural" diffusion $d(u,x) \geq 0$ and adding only that much numerical viscosity as needed for stability. The resulting adaptive viscosity scheme is an E–scheme. In Sect. 5 we prove that explicit three-point E–schemes are monotone. Applying the calculus of inverse–monotone matrices, it is shown in Sect. 6 that also implicit E–schemes are monotone. Using Kröner's version [18] of Harten's theorem [10], it follows that ϑ–time stepping with E–fluxes is a TVD operation, see Sect. 7. Numerical experiments in Sect. 9 demonstrate the effect of reduced numerical viscosity in the presence of natural diffusion. Finally, in Sect. 13 a nonlinear reaction term is included in the analysis and stability of the adaptive E–scheme when applied to balance laws is proven. Conclusions follow in Sect. 14.

The numerical analysis of possibly degenerate convection–diffusion equations has a long history. Some milestones are the following: Crandall and Majda [5] studied monotone schemes. Breuß[2, 3] presented a rigorous theory of implicit, monotone methods. Osher [21] introduced E–schemes and Tadmor [25] showed their entropy stability by comparison to the classical Godunov scheme. Even so these schemes are designed for hyperbolic conservation laws, their analysis relies on numerical viscosity. Karlsen et al. in a series of papers [7, 6, 4, 12, 13, 14] developed the theory and numerics of strongly degenerate convection–diffusion equations. In [7] they found that strongly degenerate

Received by the editors September 30, 2019 and, in revised form, March 3, 2020.
2000 *Mathematics Subject Classification.* 35K65, 35L65, 65M06, 65M08.

problems develop more complex structures than purely hyperbolic equations. A class of conservative–form difference schemes, treating the convective and diffusive flux as one effective conservative flux, is shown to converge to the unique BV entropy weak solution. Our contribution is to minimize the numerical diffusion in the effective flux (without solving nonlinear Riemann problems). In [4] Chen and Karlsen establish continuous dependence for anisotropic degenerate parabolic PDEs. Anisotropic numerical viscosity appears in finite volume schemes on unstructured grids where total variation bounds are not available. Error estimates and convergence rates are given in [12, 13, 14].

2. Preliminaries

Consider the convection–diffusion equation (1) with $f \in C^1(\mathbb{R})$, $\|f'\|_\infty < \infty$ and possibly degenerate "natural" diffusion $d(u,x) \geq 0$. Let $\epsilon\Delta x \geq 0$ denote artificial diffusion and $D = d + \epsilon\Delta x$ the effective, total diffusion. On an uniform mesh $x_j = j\Delta x$, $\Delta x > 0$ the second order central difference operator

$$-\frac{1}{\Delta x^2}\Gamma_D \approx \partial_x \left(D\partial_x\right)$$

is given by a symmetric matrix. At inner grid points it has the local structure

$$\Gamma_D \sim \begin{pmatrix} D_{j-3/2} + D_{j-1/2} & -D_{j-1/2} & \\ -D_{j-1/2} & D_{j-1/2} + D_{j+1/2} & -D_{j+1/2} \\ & -D_{j+1/2} & D_{j+1/2} + D_{j+3/2} \end{pmatrix}$$

where $D_{j+1/2} = D(x_{j+1/2})$ is evaluated at the interface $x_{j+1/2} = (j+1/2)\Delta x$. The convection term is discretized as

$$f(u)_x \approx \frac{1}{2\Delta x}\Lambda\phi(u) \ ,$$

where ϕ denotes the diagonal field $\phi(u)_j = f(u_j)$ and Λ is the anti–symmetric, central difference operator

$$\Lambda \sim \begin{pmatrix} 0 & 1 & \\ -1 & 0 & 1 \\ & -1 & 0 \end{pmatrix} \ .$$

For periodic problems it will be sufficient to consider "inner" mesh points. Applying periodic boundary conditions and identifying overlapping points the equations at the boundary are the same, see Sect. 8. Also note the finite mesh and finite dimensional discrete operators represented by finite matrices.

The convection diffusion operator $-f(u)_x + (d(u,x)u_x)_x$ is discretized by central differences

$$F_{\Delta x}(u) = -\frac{1}{\Delta x^2}\Gamma_D u - \frac{1}{2\Delta x}\Lambda\phi(u) \ .$$

The classical, central difference scheme has no artificial diffusion $\epsilon = 0$, while Lax–Friedrichs uses $\epsilon = \frac{1}{2}\frac{\Delta x}{\Delta t}$. The forward marching scheme

$$u^{n+1} = u^n + \Delta t F_{\Delta x}(u^n) = \mathcal{H}(u^n)$$

is monotone in the sense of Crandall and Majda [5] if $\mathcal{H} = I + \Delta t F_{\Delta x}$ is a non–decreasing function in all unknowns. In particular, the Jacobian $DF_{\Delta x}$ is off–diagonal non–negative, or quasi–positive.

Whenever diffusion $D = d + \epsilon\Delta x$ does not depend on u, the Jacobian reads

$$DF_{\Delta x}(u) = -\frac{1}{\Delta x^2}\Gamma_D - \frac{1}{2\Delta x}\Lambda \mathrm{diag}(f'(u))$$

and quasi–positivity is ensured by enough diffusion

$$2D_{j\pm1/2} \geq \Delta x \|f'\|_\infty \ . \tag{2}$$

Apparently, classical, central differences require enough given, natural diffusion in relation to the mesh size. The CFL condition $\frac{\Delta t}{\Delta x}\|f'\|_\infty \leq 1$ ensures that the Lax–Friedrichs scheme has enough diffusion $\epsilon\Delta x = \frac{1}{2}\frac{\Delta x^2}{\Delta t}$, even in the absence of natural diffusion.

Rusanov's local Lax–Friedrichs scheme [22] adapts the numerical viscosity locally

$$\epsilon_{j+1/2} = \frac{1}{2}\max_u |f'(u)| \ , \quad \forall u \in \overline{u_j, u_{j+1}} \tag{3}$$

such that $\epsilon = \epsilon(u)$ and hence $D = D(u)$ do depend on u. In this case monotonicity is not discussed as easily by taking derivatives. However, as E–scheme, also local Lax–Friedrichs is monotone, see Sect. 5.

3. An adaptive viscosity E–scheme

To be on the safe side, Lax–Friedrichs applies artificial diffusion enough to approximate inviscid conservation laws disregarding any available, natural viscosity. In fact, the scheme is designed for hyperbolic problems. Classical central differences, on the other hand, need positive natural diffusion and fine meshes. They cannot deal with locally degenerate viscosity and become unstable in the limit $d \to 0$. When dealing with diffusive conservation laws, it is therefore tempting to adopt the artificial viscosity to the characteristic speed of the hyperbolic operator $f'(u)$ and the available natural diffusion $d(u, x) \geq 0$. To satisfy the "enough diffusion" condition (2) it is sufficient to set

$$\epsilon_{j+1/2} = \max\left(0, \frac{1}{2}|f'|_{j+1/2} - \frac{1}{\Delta x}d_{j+1/2}\right) \ , \tag{4}$$

where $d_{j+1/2}$ means $d(\bar{u}_{j+1/2}, x_{j+1/2})$ with $\bar{u}$ the average $\bar{u}_{j+1/2} = (u_j + u_{j+1})/2$ and $x_{j+1/2} = (j + 1/2)\Delta x$ while $|f'|_{j+1/2}$ denotes the local maximum

$$|f'|_{j+1/2} = \max_u |f'(u)| \ , \quad \forall u \in \overline{u_j, u_{j+1}} \ .$$

Note that this choice avoids artificial anti–diffusion $\epsilon \geq 0$ and guarantees the local condition

$$2D_{j+1/2} \geq \Delta x |f'|_{j+1/2} \ . \tag{5}$$

The adaptive Lax–Friedrichs flux

$$F(u_j, u_{j+1}) = \frac{1}{2}\left(f(u_j) + f(u_{j+1})\right) - \frac{D_{j+1/2}}{\Delta x}\left(u_{j+1} - u_j\right) \tag{6}$$

with

$$D_{j+1/2} = d_{j+1/2} + \epsilon_{j+1/2}\Delta x \tag{7}$$

and ϵ according to (4) is consistent with the viscous conservation law (1) in the sense that $F(u, u) = f(u)$. It is not difficult to verify that the adaptive viscosity scheme is an E–scheme. According to Osher [21], a three point scheme in conservation form

$$u_j^{n+1} = u_j^n - \frac{\Delta t}{\Delta x}\left(F(u_j^n, u_{j+1}^n) - F(u_{j-1}^n, u_j^n)\right) \tag{8}$$

is called E–scheme if its flux satisfies the E–property

$$\text{sign}(u_{j+1} - u_j)\left(F(u_j, u_{j+1}) - f(u)\right) \leq 0 \ , \quad \forall u \in \overline{u_j, u_{j+1}} \ . \tag{9}$$

A flux satisfying (9) is also called E–flux.

Lemma 3.1. *The numerical flux (6) with sufficient diffusion (5) is an E–flux.*

Proof. Assume $u_j \le u \le u_{j+1}$ and find

$$\begin{aligned} f(u_{j+1}) &= f(u) + f'(\xi)(u_{j+1} - u) \ , \quad \xi \in [u, u_{j+1}] \\ f(u_j) &= f(u) - f'(\eta)(u - u_j) \ , \quad \eta \in [u_j, u] \ . \end{aligned}$$

Using (5)

$$\begin{aligned} \frac{1}{2}\left(f(u_j) + f(u_{j+1})\right) &= f(u) + \frac{1}{2}f'(\xi)(u_{j+1} - u) - \frac{1}{2}f'(\eta)(u - u_j) \\ &\le f(u) + \frac{D_{j+1/2}}{\Delta x}(u_{j+1} - u) + \frac{D_{j+1/2}}{\Delta x}(u - u_j) \\ &= f(u) + \frac{D_{j+1/2}}{\Delta x}(u_{j+1} - u_j) \ . \end{aligned}$$

By definition of the flux (6) the E–property (9) follows. The remaining other case $u_j \ge u \ge u_{j+1}$ is analogous. □

As (4) implies (5) it is clear that

Corollary 3.2. *The central scheme (6) (7) and (8) with numerical viscosity adapted by (4) is E–scheme.*

Note, the condition for monotonicity (5) is sharp. Without natural diffusion d the numerical diffusion ϵ cannot be reduced and the adaptive scheme coincides with local Lax–Friedrichs. The adaptive E–scheme develops its potential in the presence of limited, variable and degenerate diffusion $d \ge 0$. With positive diffusion $d > 0$ and fine meshes $\Delta x \ll 1$ on the other hand, less artificial diffusion is required by (4) and the gain in resolution by the adaptive scheme is less. See also the numerical experiments in Sect. 9.

4. Strongly degenerate problems and conservative differencing

Following Evje and Karlsen [7] the non–linear convection–diffusion equation

$$u_t + f(u)_x = (d(u)u_x)_x \ , \quad d(u) \ge 0 \tag{10}$$

is called strongly degenerate if d vanishes on a non–trivial interval

$$d(u) = 0 \ , \quad \forall u \in [\alpha, \beta] \ , \quad \alpha < \beta \ .$$

In that case the solution to the Cauchy problem is more complex than solutions to hyperbolic conservation laws and naive schemes fail to capture the entropy weak solution. The cure to the problem is conservative differencing of the total flux as follows. Denote by $k(u)$ the primitive

$$k(u) = \int_0^u d(s)\ \mathrm{d}s$$

and rewrite the PDE (10) in conservative form

$$u_t + (f(u) - k(u)_x)_x = 0 \ .$$

Approximate the total flux $f(u) + k(u)_x$ for example by the augmented Lax–Friedrichs formula

$$\begin{aligned} F(u_j, u_{j+1}) &= \frac{1}{2}\left(f(u_j) + f(u_{j+1})\right) - \epsilon_{j+1/2}\left(u_{j+1} - u_j\right) \\ &\quad - \frac{1}{\Delta x}\left(k(u_{j+1}) - k(u_j)\right) \end{aligned} \tag{11}$$

and apply conservative differencing (8).

Note that $k(u_{j+1}) - k(u_j) = d(\xi)\,(u_{j+1} - u_j)$ for some $\xi \in \overline{u_j, u_{j+1}}$. With adaptive numerical viscosity

$$\epsilon_{j+1/2} = \max\left(0, \frac{1}{2}|f'|_{j+1/2} - \frac{1}{\Delta x}\min(d)_{j+1/2}\right) \ ,$$

where $\min(d)_{j+1/2}$ is the local minimum

$$\min(d)_{j+1/2} = \min_u d(u) \ , \quad \forall u \in \overline{u_j, u_{j+1}} \ ,$$

the effective diffusion

$$D_{j+1/2} = d(\xi) + \epsilon_{j+1/2}\Delta x \geq \frac{1}{2}|f'|_{j+1/2}$$

is enough to make an E–flux, see Lemma 3.1. In Section 9 below it is demonstrated that this conservative E–scheme approximates the entropy weak solution at improved resolution.

5. Three–point E–schemes are monotone

A three–point scheme in conservation form (8) is monotone if

$$H(u_{j-1}, u_j, u_{j+1}) = u_j - \frac{\Delta t}{\Delta x}\left(F(u_j, u_{j+1}) - F(u_{j-1}, u_j)\right)$$

is non–decreasing in all its arguments [5]. By setting $f(u) = F(u, u)$ in the E–condition (9) it is obvious that a monotone and consistent scheme (8) is E–scheme. To show that consistent E–schemes are monotone, consider first

Lemma 5.1. *A consistent, three point E–scheme (8), (9) is quasi–monotone; that is* $\partial_v F(v, w) \geq 0$ *and* $\partial_w F(v, w) \leq 0$.

Proof. Assume $u_j < u_{j+1}$. By the E–property (9)

$$F(u_j, u_{j+1}) \leq f(u) \ , \quad \forall u \in [u_j, u_{j+1}] \ .$$

Selecting $u = u_{j+1}$:

$$F(u_j, u_{j+1}) \leq f(u_{j+1}) = F(u_{j+1}, u_{j+1}) \ .$$

We find that $F(v, w)$ is non–decreasing in v. Choosing $u = u_j$ instead:

$$F(u_j, u_{j+1}) \leq f(u_j) = F(u_j, u_j) \ .$$

Apparently $F(v, w)$ is non–increasing in w. Similar arguments in the case $u_j > u_{j+1}$ complete the proof. □

Lemma 5.2. *If* $\partial_v F(v, w) \geq 0$, $\partial_w F(v, w) \leq 0$ *and the CFL–condition holds*

$$\frac{\Delta t}{\Delta x}\|\partial_v F - \partial_w F\|_\infty \leq 1 \ , \tag{12}$$

then the scheme (8) is monotone.

Proof.

$$\partial_{u_{j-1}} H(u_{j-1}, u_j, u_{j+1}) = \frac{\Delta t}{\Delta x}\partial_{u_{j-1}} F(u_{j-1}, u_j) \geq 0 \ .$$

$$\partial_{u_{j+1}} H(u_{j-1}, u_j, u_{j+1}) = -\frac{\Delta t}{\Delta x}\partial_{u_{j+1}} F(u_j, u_{j+1}) \geq 0 \ .$$

The CFL–condition (12) ensures that

$$\partial_{u_j} H(u_{j-1}, u_j, u_{j+1}) = 1 - \frac{\Delta t}{\Delta x}\left(\partial_{u_j} F(u_j, u_{j+1}) - \partial_{u_j} F(u_{j-1}, u_j)\right) \geq 0 \ .$$

This completes the proof. □

The main result of this section is an obvious consequence of Lemma 5.1 and Lemma 5.2:

Corollary 5.3. *A consistent, three–point E–scheme (8), (9) is monotone if the CFL–condition (12) holds.*

Finally, the adaptive viscosity scheme as E–scheme is also monotone:

Corollary 5.4. *Under the CFL–condition (12), the adaptive viscosity scheme (7, 8, 6, 4) is monotone.*

6. Implicit time stepping

As diffusive problems tend to be stiff, it is appropriate to consider implicit time stepping applied to the semi–discrete system $u_t = F_{\Delta x}(u)$. The discretization in space is conservative

$$F_{\Delta x}(u)_j = -\frac{1}{\Delta x}\left(F_{j+1/2} - F_{j-1/2}\right) \ , \quad F_{j+1/2} = F(u_j, u_{j+1}) \tag{13}$$

with a consistent E–flux (9). For such systems, consider ϑ–time stepping

$$\frac{1}{\Delta t}\left(u^{n+1} - u^n\right) = \vartheta F_{\Delta x}(u^{n+1}) + (1-\vartheta)F_{\Delta x}(u^n) \ , \quad 0 \le \vartheta \le 1 \ . \tag{14}$$

The parameter ϑ determines the method: $\vartheta = 0/0.5/1$ corresponds to explicit Euler / Crank–Nicholson / implicit Euler, respectively. Sorting out next and previous time levels

$$\frac{1}{\Delta t}u^{n+1} - \vartheta F_{\Delta x}(u^{n+1}) = \frac{1}{\Delta t}u^n + (1-\vartheta)F_{\Delta x}(u^n)$$

we define the left– and right–hand side operators

$$L_h(u) = \frac{1}{\Delta t}u - \vartheta F_{\Delta x}(u) \ , \quad R_h(u) = \frac{1}{\Delta t}u + (1-\vartheta)F_{\Delta x}(u) \ .$$

To investigate the monotonicity of the implicit ϑ–scheme, consider two solutions u and v:

$$L_h(u^{n+1}) - L_h(v^{n+1}) = R_h(u^n) - R_h(v^n) \ .$$

Let

$$C^n_{\Delta x} = \int_0^1 DF_{\Delta x}(v^n + s(u^n - v^n))\,\mathrm{d}s \ ,$$

$$A^n_h = \frac{1}{\Delta t}I - \vartheta C^n_{\Delta x} \ , \quad B^n_h = \frac{1}{\Delta t}I + (1-\vartheta)C^n_{\Delta x} \ .$$

It follows

$$A^n_h(u^{n+1} - v^{n+1}) = B^n_h(u^n - v^n) \ .$$

By Lemma 5.1 the Jacobian $DF_{\Delta x}$ thus $C^n_{\Delta x}$ and B^n_h are quasi–positive while A^n_h is Z–matrix. For Δt small enough

$$(1-\vartheta)\,\frac{\Delta t}{\Delta x}\|\partial_v F - \partial_w F\|_\infty \le 1 \ , \tag{15}$$

B^n_h is non–negative. Due to the conservation form (13), the Jacobian shows the local structure $DF_{\Delta x} \sim$

$$-\frac{1}{\Delta x}\begin{pmatrix} \partial_v F_{j-1/2} - \partial_w F_{j-3/2} & \partial_w F_{j-1/2} & \\ -\partial_v F_{j-1/2} & \partial_v F_{j+1/2} - \partial_w F_{j-1/2} & \partial_w F_{j+1/2} \\ & -\partial_v F_{j+1/2} & \partial_v F_{j+3/2} - \partial_w F_{j+1/2} \end{pmatrix} \ .$$

It is obvious that inner columns (in contrast to rows), sum to zero. Taking into account boundary conditions, see Sect. 8, we find $DF^T_{\Delta x}\delta \leq 0$. Here $\delta = (1, 1, \dots 1)^T$ denotes the vector of ones. It follows $(C^n_{\Delta x})^T\delta \leq 0$ and

$$(A^n_h)^T\delta \geq \frac{1}{\Delta t} > 0 \ .$$

By the M–criterion (Bohl [1], Theorem I.4.3 or Fiedler and Pták [8] Theorem (4,3)) A^n_h is M–matrix i.e. $(A^n_h)^{-1} \geq 0$. Finally, also implicit E–schemes are monotone in the sense:

$$u^{n+1} - v^{n+1} \geq \left(A^{n+1}_h\right)^{-1} B^n_h(u^n - v^v) \ , \quad \left(A^{n+1}_h\right)^{-1} B^n_h \geq 0 \ .$$

If initially $u^0 \geq v^0$ (componentwise for all j), then the same is true at later time.

Lemma 6.1. *Under the time step restriction (15) ϑ–time stepping (14) for a consistent and conservative (8) E–flux (9) is a monotone operation.*

It is well–known that monotone methods are total variation diminishing (TVD). In the next section, we present a direct approach to TVD.

7. E–schemes are TVD

Applying Harten's theorem [10] we shall see that the CFL–condition guarantees R_h to be a TVD operator. Moreover, Kröner's extension of Harten's theorem turns L_h into a total variation increasing (TVI) operator. Consequently the ϑ–scheme $L_h(u^{n+1}) = R_h(u^n)$ is TVD for any value of $\vartheta \in [0, 1]$.

Theorem 7.1 (Harten). *The method*

$$u^{n+1}_j = u^n_j + \alpha_{j+1/2}\left(u^n_{j+1} - u^n_j\right) - \beta_{j-1/2}\left(u^n_j - u^n_{j-1}\right)$$

is TVD if $\alpha_{j+1/2} \geq 0$, $\beta_{j-1/2} \geq 0$ and $\alpha_{j+1/2} + \beta_{j+1/2} \leq 1$.

Corollary 7.2. *Let $F(v, w)$ be a consistent, Lipschitz continuous*

$$\left.\begin{matrix} F(v,w) - f(w) \\ F(v,w) - f(v) \end{matrix}\right\} \geq -L(w - v) \tag{16}$$

E–flux (9). Under the CFL–condition

$$(1 - \vartheta)\frac{\Delta t}{\Delta x}2L \leq 1 \tag{17}$$

R_h is a TVD operator: $TV(R_h(u)) \leq TV(u)$.

Proof. The E–condition (9) implies the flux to be quasi–monotone, see Lemma 5.1 i.e. $\partial_u F(u, v) \geq 0$ and $\partial_v F(u, v) \leq 0$. Hence,

$$C_{j+1/2} = \frac{F(u_j, u_{j+1}) - f(u_j)}{u_{j+1} - u_j} \leq 0 \ ,$$

$$E_{j+1/2} = \frac{F(u_j, u_{j+1}) - f(u_{j+1})}{u_{j+1} - u_j} \leq 0 \ ,$$

and $C_{j+1/2} + E_{j+1/2} \geq -2L$. By definition

$$\left[\Delta t R_h(u)\right]_j = u_j + \alpha_{j+1/2}\left(u_{j+1} - u_j\right) - \beta_{j-1/2}\left(u_j - u_{j-1}\right)$$

with

$$\alpha_{j+1/2} = -(1 - \vartheta)\frac{\Delta t}{\Delta x}C_{j+1/2} \geq 0 \ ,$$

$$\beta_{j+1/2} = -(1 - \vartheta)\frac{\Delta t}{\Delta x}E_{j+1/2} \geq 0 \ ,$$

and $\alpha_{j+1/2} + \beta_{j+1/2} \leq (1 - \vartheta)\frac{\Delta t}{\Delta x}2L \leq 1$. The claim follows by Theorem 7.1. □

Using the same coefficients $C_{j+1/2}$ and $E_{j+1/2}$ the left–hand side reads

$$[\Delta t L_h(u)]_j = u_j + \widetilde{\alpha}_{j+1/2}\,(u_{j+1} - u_j) - \widetilde{\beta}_{j-1/2}\,(u_j - u_{j-1})$$

with non–positive coefficients

$$\begin{aligned}\widetilde{\alpha}_{j+1/2} = \vartheta\frac{\Delta t}{\Delta x}C_{j+1/2} &\leq 0\ ,\\ \widetilde{\beta}_{j+1/2} = \vartheta\frac{\Delta t}{\Delta x}E_{j+1/2} &\leq 0\ .\end{aligned}$$

A direct application of Kröner's lemma ([18] Lemma 2.3.20) shows that L_h is a TVI operator.

Lemma 7.3 (Kröner). *Consider*

$$u_j^{n+1} = u_j^n + \alpha_{j+1/2}\left(u_{j+1}^n - u_j^n\right) - \beta_{j-1/2}\left(u_j^n - u_{j-1}^n\right)\ .$$

If $\alpha_{j+1/2} \leq 0$ *and* $\beta_{j-1/2} \leq 0$, *then* $TV(u^{n+1}) \geq TV(u^n)$.

It follows that the ϑ–scheme is TVD:

Corollary 7.4. *Assume F is a consistent, Lipschitz continuous (16) E–flux (9). Given the CFL–condition (17) the ϑ–scheme $L_h(u^{n+1}) = R_h(u^n)$ is TVD.*

Proof. $TV(u^{n+1}) \leq TV(L_h(u^{n+1})) = TV(R_h(u^n)) \leq TV(u^n)$. □

8. Boundary conditions

What type of boundary condition to pose with the multiphysics PDE (1) depends on the local type of the PDE. In case of periodic data it is appropriate to ask for periodic solutions thus avoiding the identification of specific boundary conditions. For example, assuming 1–periodic initial data $u(0,x) = u(0,1+x)$ and diffusion coefficients $d(u,x) = d(u,1+x)$, the 1–periodic solution is to be determined on the mesh

$$x_j = j\Delta x\ ,\quad \Delta x = \frac{1}{M}\ ,\quad j = 1,2,\ldots,M\ .$$

Identifying u_{M+j} with u_j the conservative space discretization (13) reads

$$F_{\Delta x}(u) = -\frac{1}{\Delta x}\begin{pmatrix} F(u_1,u_2) - F(u_M,u_1) \\ F(u_j,u_{j+1}) - F(u_{j-1},u_j)\ ,\quad j = 2,3\ldots M-1 \\ F(u_M,u_1) - F(u_{M-1},u_M)\end{pmatrix}\ .$$

Due to the conservation form, inner columns of the Jacobian sum to zero. By periodicity $u_0 = u_M$ and the first column

$$-\frac{1}{\Delta x}\left(F_v(u_1,u_2) - F_w(u_M,u_1), -F_v(u_1,u_2), 0\cdots 0, F_w(u_M,u_1)\right)^T$$

sums to zero. Similarly the last column sums to zero and $DF(u)^T_{\Delta x}\delta = 0$. By Lemma 5.1 for consistent E–schemes the Jacobian is quasi–positive. Monotonicity follows along the lines in Sect. 6.

For parabolic boundaries, for example when $d(u,0) > 0$ at the left boundary, also Dirichlet conditions are common. In that case $u(t,0) = u_0 = \gamma$ is given and the space discretization reduces to

$$F_{\Delta x}(u) = -\frac{1}{\Delta x}\begin{pmatrix} F(u_1,u_2) - F(\gamma,u_1) \\ F(u_2,u_3) - F(u_1,u_2) \\ \vdots\end{pmatrix}\ .$$

Apparently the Jacobian is quasi–positive

$$-\frac{1}{\Delta x}\begin{pmatrix} F_v(u_1,u_2)-F_w(\gamma,u_1) & F_w(u_1,u_2) & \\ -F_v(u_1,u_2) & F_v(u_2,u_3)-F_w(u_1,u_2) & F_w(u_2,u_3) \\ \ddots & \ddots & \ddots \end{pmatrix} .$$

Columns sum to zero except the first column where the sum is short of one term

$$\left(DF_{\Delta x}^T\delta\right)_1 = \frac{1}{\Delta x}F_w(\gamma,u_1) \le 0 \ .$$

Again $DF_{\Delta x}^T\delta \le 0$ and monotonicity follows.

Without diffusion $d(0) = 0$ or for a homogenous Neumann condition $u(t,0)_x = 0$ the boundary is hyperbolic and well posedness of the initial boundary value problem is nontrivial, see [9, 16, 17]. In this situation the in–going characteristics need to be specified.

9. Numerical experiments

This first example is constructed to demonstrate the effect of reduced artificial diffusion. Consider the viscous advection equation

$$u_t + u_x = (d(x)u_x)_x \tag{18}$$

with degenerate diffusion

$$d(x) = \max\left(0, \frac{1}{40}\cos\left(\frac{\pi x}{6}\right)\right) \tag{19}$$

and initial data $u|_{t=0} = \chi_{[-4,-3]\cup[-2,-1]}$. Approximate solutions are computed on the interval $[-6,6]$ using a mesh size of $\Delta x = 1/20$ and applying periodic boundary conditions.

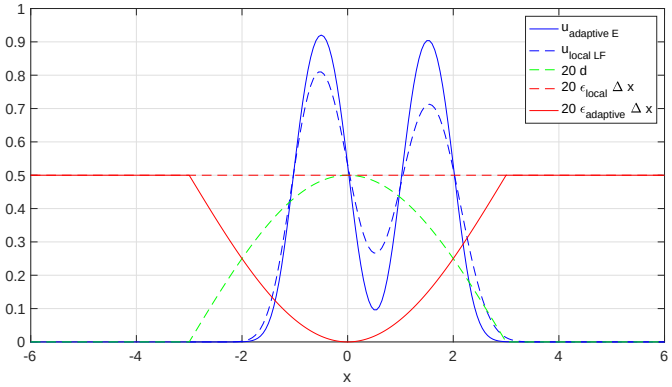

FIGURE 1. Approximations to (18) at $t = 3$ with given–, local and adaptive viscosities, $\Delta x = 1/20$, CFL=0.8.

Approximations generated by the local Lax–Friedrichs scheme in comparison to the adaptive viscosity method are displayed in Fig. 1. Explicit Euler time stepping is applied. By Corrolary 5.4 the time step should be limited by (12). With local and adaptive viscosity coefficients however, the partial derivatives $\partial_v F$ and $\partial_w F$ may be complicated. A good practical compromise is to limit

$$\frac{\Delta t}{\Delta x^2}\max_j\left(D_{j+1/2}+D_{j-1/2}\right) = \mathrm{CFL} \ , \tag{20}$$

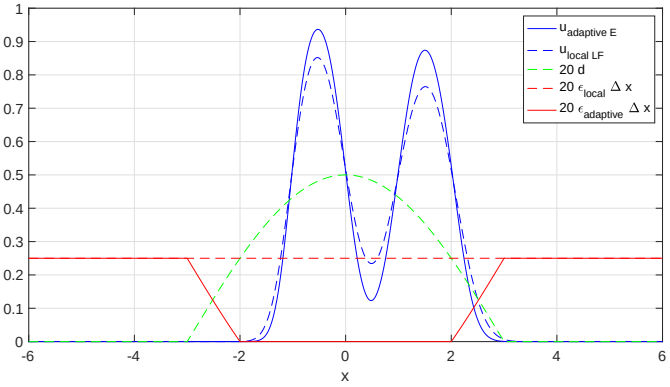

FIGURE 2. Approximations to (18) at $t = 3$ on refined mesh $\Delta x = 1/40$, CFL=0.8.

with a CFL number less that one. With constant characteristic speed $f'(u) = 1$ local Lax–Friedrichs applies constant artificial viscosity $2\epsilon_l = 1$ according to (3) and disregarding any given viscosity. The adaptive scheme however, reduces artificial diffusion where natural diffusion is available. This leads to less effective diffusion $D = d + \epsilon\Delta x$ and reduced damping, see Fig. 1.

Artificial viscosities scale with the mesh size. On a refined mesh $\Delta x = 1/40$ the adaptive scheme does not require any artificial viscosity for $x \in [-2, 2]$, see Fig. 2.

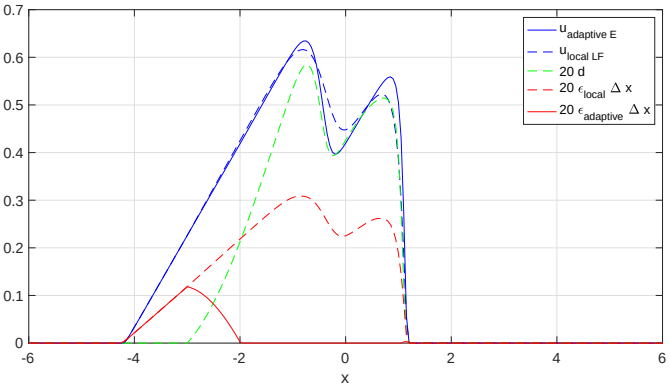

FIGURE 3. Approximations to Burgers' equation (21) at time $t = 5$, $\Delta x = 1/20$, CFL=0.8.

A test with the fully nonlinear viscous Burgers' equation

$$u_t + \frac{1}{2}(u^2)_x = (d(u,x)u_x)_x \quad , \quad d(u,x) = \max\left(0, \frac{u}{20}\cos\left(\frac{\pi x}{6}\right)\right) \tag{21}$$

demonstrates the stability and superior accuracy of the adaptive E–scheme. Note the solution dependent natural diffusion in Fig. 3.

As expected, the difference between both schemes measured in L^1–norm scales linearly with the mesh size. Table 1 confirms that both schemes converge to the same solution.

The next test case is a degenerate convection–diffusion equation

$$u_t + f(u)_x = (d(u)u_x)_x \tag{22}$$

TABLE 1. L^1 deviation between local Lax–Friedrichs and adaptive E–schemes applied to advection (18) (left) and Burgers' equation (21) (right).

Δx	L^1 difference	rate
1/20	0.40451	-
1/40	0.27122	0.58
1/80	0.14990	0.86
1/160	0.07991	0.91
1/320	0.04151	0.94

Δx	L^1 difference	rate
1/20	0.084450	-
1/40	0.045939	0.88
1/80	0.023048	1.00
1/160	0.011570	0.99
1/320	0.005797	1.00

with convective Burgers flux and strongly degenerate diffusion

$$d(u) = 0.05 \max(0, u^2 - 0.25^2) \ .$$

Initial data is a step function $u|_{t=0} = \chi_{[-4,-2]} + 0.7\chi_{[0,1]}$. The solution is a pair of shocks and rarefaction waves where the second pair is faster, catches up and interacts with the slower pair ahead. The mesh size is $\Delta x = 1/20$ with CFL number 1.0. Fig. 4 displays approximations by the conservative E–scheme (11), (8) at time $t = 5$. Note that for increasing d the local minimum $\min(d)_{j+1/2}$ is easily evaluated as $\min(d)_{j+1/2} = d(\min(u_j, u_{j+1}))$. Observe the strongly degenerate diffusion for $u < 0.25$ and the effect of the adaptive numerical viscosity.

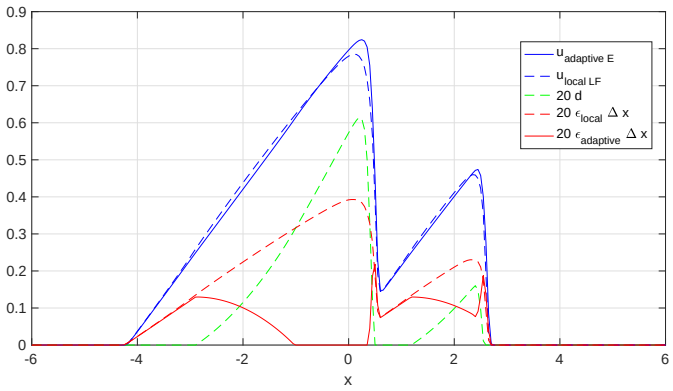

FIGURE 4. Approximation to the strongly degenerate problem (10) at $t = 5$, $\Delta x = 1/20$, CFL=1.0

To confirm that our scheme finds the entropy weak solution, we recompute the case by Evje and Karlsen [7] with Burgers type flux $f(u) = u^2$ and piecewise linear diffusion

$$d(u) = \begin{cases} 0 & \text{for } 0 \le u \le 0.5 \\ 2.5u - 1.25 & \text{for } 0.5 < u < 0.6 \\ 0.25 & \text{for } 0.6 \le u \end{cases}$$

The approximation features the desired increasing shock located at $x \approx 0.4$, see Fig. 5. Instead of extremely fine meshes, we apply minmod slopes as described in Section 10 with step–size $\Delta x = 1/320$ and CFL=0.5.

In the next experiment we approximate the solution to the conservation law

$$u_t + \nabla \cdot f(u) = \nabla \cdot (d(x)\nabla u) \quad , \quad f(u) = \left(u^2/2, u^4/4\right)^T \tag{23}$$

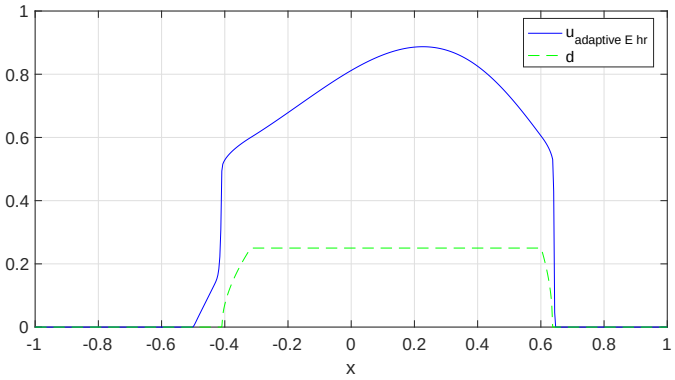

FIGURE 5. Approximation to the strongly degenerate problem (10) at $t = 0.15$, $\Delta x = 1/320$, CFL=0.5

TABLE 2. Piecewise constant initial data.

-1.0	+1.0	-1.5	+1.0
+1.5	-0.5	+1.5	-0.5

in two variables $|x| \leq 10$ and $|y| \leq 6$. The viscosity coefficient depends on x alone. It is largest around $x = 0$ and fades out towards the left and right boundaries.

$$d(x) = \max\left(0, \frac{1}{40}\left(\frac{1}{2} + \sin\left(\frac{\pi(x+5)}{10}\right)\right)\right) \quad .$$

Initial data is piecewise constant. In square blocks of size 4×4 units, the data shown in Tab. 2 is given. In the background, the u–value is zero. Finally, boundary conditions are periodic in both variables.

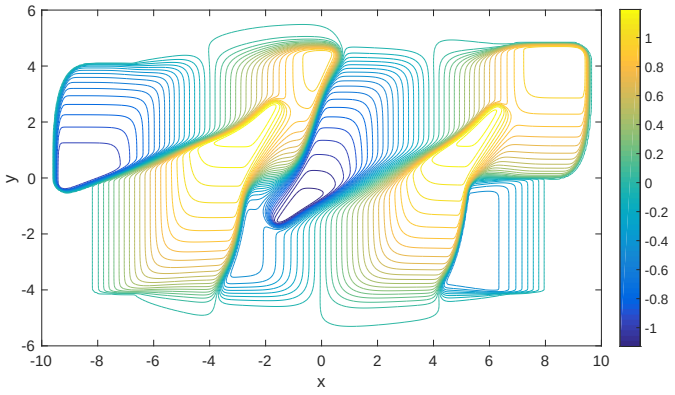

FIGURE 6. Approximation to (23) by the adaptive E–scheme at $t = 3$, $\Delta x = \Delta y = 1/20$, CFL=0.5.

The one dimensional schemes are applied in both coordinate directions. Approximations are advanced in time by an explicit Euler step. The time–step is limited by (20) applied to both directions and with a CFL limit of 0.5.

The approximation by the adaptive E–scheme on a 400×240 points mesh is displayed in Fig. 6. A cross–section along the line $y = -1.3$ reveals large differences around $x = -1$,

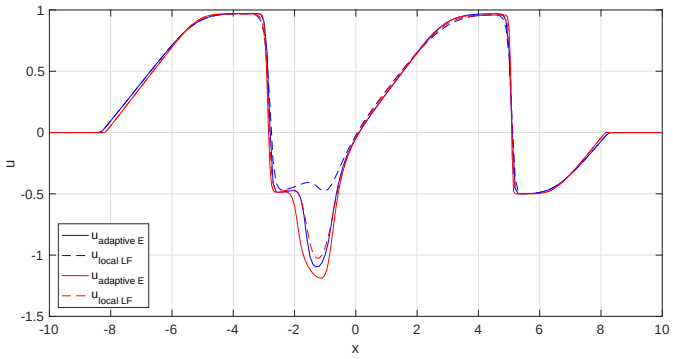

FIGURE 7. Cross–section at $y = -1.3$, $t = 3$, $\Delta x = \Delta y = 1/10$ (blue) and $\Delta x = \Delta y = 1/20$ (red).

see Fig 7. While the adaptive scheme resolves the minimum already on the coarse grid, local Lax–Friedrichs can only hardly sense it. Mesh refinement confirms the location of the minimum. Apparently both schemes converge to the same solution.

10. A relaxed, high resolution adaptive viscosity E–scheme

Adaptive viscosity E–schemes develop their potential in the presence of natural diffusion. In inviscid, purely hyperbolic regions, high resolution may be achieved using TVD reconstructions [19]. For systems of conservation laws however, the conserved variables are nonlinearly coupled and do not obey the TVD principle. Therefore it is questionable to apply TVD reconstructions to conserved variables. The relaxation approximation [11] provides an alternative approach:

$$\begin{aligned} u_t + v_x &= 0 \\ v_t + a^2 u_x &= \frac{1}{b}\left(f(u) - v\right) \quad . \end{aligned} \tag{24}$$

Under the sub–characteristic condition $a \geq \|f'\|_\infty$ Natalini [20] proved convergence towards the solution of the nonlinear hyperbolic conservation law $u_t + f(u)_x = 0$ as $b \to 0$.

The interesting aspect of the relaxation system is that the nonlinear flux function appears as a stiff source term, but not in the PDE operator. The latter is a linear advection system with characteristic variables

$$(v \pm au)_t \pm a(v \pm au)_x = 0 \quad . \tag{25}$$

The solution of the Riemann problem is the left and right state, respectively

$$\begin{aligned} (v + au)_{j+1/2} &= (v + au)_j \\ (v - au)_{j+1/2} &= (v - au)_{j+1} \quad . \end{aligned}$$

Especially v on the interface is the average of both characteristic variables

$$v_{j+1/2} = \frac{1}{2}\left(v_j + v_{j+1}\right) - \frac{a}{2}\left(u_{j+1} - u_j\right) \quad .$$

The stiff ODE on the right hand side of (24) is solved by Duhamel's principle: u is constant and v exponentially decays to $f(u)$. In a fractional step approach, we set $v_j^n = f(u_j^n)$ and obtain the Lax–Friedrichs flux with numerical viscosity $\epsilon = \frac{1}{2}\frac{\Delta x}{\Delta t} = \frac{a}{2}$

$$f(u)_{j+1/2}^n = \frac{1}{2}\left(f(u_j^n) + f(u_{j+1}^n)\right) - \frac{a}{2}\left(u_{j+1}^n - u_j^n\right) \quad .$$

Note that the sub–characteristic condition $a \geq \|f'\|_\infty$ with $a = \frac{\Delta x}{\Delta t}$ is equivalent to the CFL–condition $\frac{\Delta t}{\Delta x}\|f'\|_\infty \leq 1$. The local Lax–Friedrichs flux is obtained by using a variable advective speed $a_{j+1/2} = 2\epsilon_{j+1/2} = |f'|_{j+1/2}$, see (3). So–called relaxed high–resolution schemes, based on TVD–reconstructions of the characteristic variables (25), are described in the papers [23, 24].

Given a system of viscous conservation laws

$$u_t + f(u)_x = (d(x,u)u_x)_x$$

with diagonal and non–negative diffusion matrix $d = \text{diag} \geq 0$ the adaptive E–scheme applies as follows: In each computational cell C_j the propagation speed of the fastest wave, that is the largest eigenvalue $\lambda_{\max}$ of Df, is determined

$$|\lambda_{\max}|_{j+1/2} = \max_{l=j,j+1}(\max|\lambda| : \det(Df(u_l) - \lambda I) = 0) \ .$$

The relaxation parameter defining the artificial viscosity is componentwise adapted to the available natural diffusion

$$a_{j+1/2} = 2\epsilon_{j+1/2} = \max(0, |\lambda_{\max}|_{j+1/2} I - d_{j+1/2}) \ .$$

Recall $d_{j+1/2} = d(x_{j+1/2}, \bar{u}_{j+1/2})$ with $\bar{u}_{j+1/2} = (u_j + u_{j+1})/2$ and note that both $\lambda_{\max}$ and d depend on u and thus on space and time. In both adjacent cells $C_j = (x_{j-1/2}, x_{j+1/2})$ and C_{j+1} the characteristic variables $w^\pm = f(u) \pm a_{j+1/2}u$ are reconstructed by linear TVD slopes σ_j^+ and σ_{j+1}^-. At the common interface $x_{j+1/2}$ we find

$$\begin{aligned} w^+_{j+1/2} &= f(u_j) + a_{j+1/2}u_j + \sigma_j^+(x_{j+1/2} - x_j) \ , \\ w^-_{j+1/2} &= f(u_{j+1}) - a_{j+1/2}u_{j+1} + \sigma_{j+1}^-(x_{j+1/2} - x_{j+1}) \ . \end{aligned}$$

As above, the relaxed, high–resolution FV flux is obtained as average

$$f(u^n)_{j+1/2} = \frac{1}{2}(f(u_j^n) + f(u_{j+1}^n)) - \frac{a^n_{j+1/2}}{2}\left(u^n_{j+1} - u^n_j\right) - \frac{\Delta x}{4}\left(\sigma^-_{j+1} - \sigma^+_j\right)$$

but augmented by the second order central difference for the natural diffusion

$$F^n_{j+1/2} = f(u^n)_{j+1/2} - \frac{d^n_{j+1/2}}{\Delta x}\left(u^n_{j+1} - u^n_j\right) \ .$$

As the TVD limited slopes depend on discrete lateral gradients, the resulting finite volume scheme lives on a five–point stencil and the CFL limit is 1/2. For scalar problems it is TVD but not monotone and therefore not limited to first order accuracy.

11. Testing the high resolution adaptive E–scheme

Fig. 8 depicts the high resolution scheme with Koren slope limiter [15] applied to the viscous advection equation (18) (19). Both the initial condition and mesh size are as in Sec. 9, except the CFL number which is set to 0.4. As expected, the hr–scheme gives the sharpest result with least numerical damping. The interested reader may observe that the (native) adaptive E–scheme does not resolve viscous effects below the stability limit $0.5|f'|_{j+1/2}\Delta x$. In this example the effective total diffusion $D = d + \epsilon\Delta x = 0.5$ is constant. That is why for the adaptive E–scheme both peaks appear at the same hight. The high resolution scheme however, resolves the local effect and damps the second peak less. The same effect is seen by reducing the mesh size in Fig. 2.

The next experiment is to demonstrate the resolution of small variations in diffusion in Burgers' equation. Let $d(x) = (0.6 - \cos(x\pi/6))/40$ and consider the positive part (solid green) or the absolute value (dashed green) in Fig. 9. Note that the difference of both coefficients is below the stability threshold 1/80. The initial condition is $u(0,x) = (1.0 - \sin(x\pi/6))/2.0$. In solid blue we see the approximation by the hr–scheme with

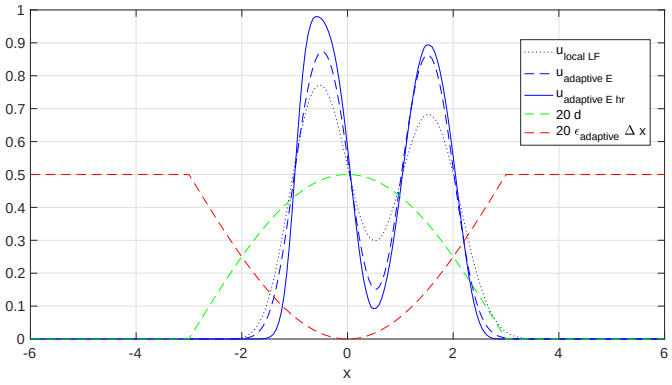

FIGURE 8. Approximations to advection equation at $t = 3.0$, $\Delta x = 1/20$, CFL=0.4.

diffusion coefficient in solid green. The difference to the dashed green coefficient is scaled up and plotted in cyan. We conclude that in contrast to the native adaptive E–scheme, the high resolution version can detect small variations in diffusion coefficients.

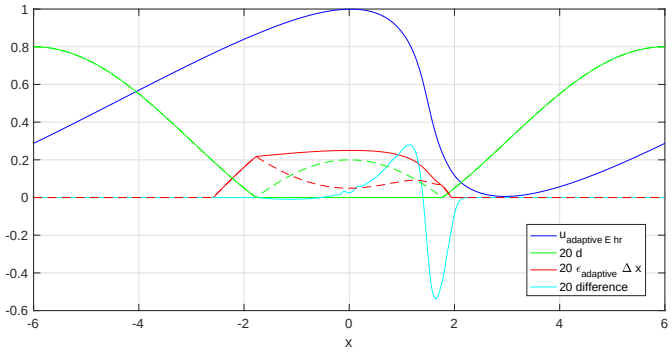

FIGURE 9. Approximations to Burgers' equation at $t = 3.0$, $\Delta x = 1/40$, CFL=0.4.

12. High resolution adaptive E–schemes in gas dynamics

The Navier–Stokes equations [17] describe conservation of mass

$$\rho_t + \nabla \cdot (\rho \mathbf{u}) = 0 \ , \tag{26}$$

and momentum

$$\frac{\mathrm{D}}{\mathrm{D}t}(\rho \mathbf{u}) + \rho \mathbf{u} \nabla \cdot \mathbf{u} + \nabla p = \nabla \cdot \sigma \ .$$

Here ρ and $\rho \mathbf{u}$ denote mass– and momentum densities respectively. $\mathrm{D}/\mathrm{D}t$ is the material derivative $\mathrm{D}f/\mathrm{D}t = \partial f/\partial t + \mathbf{u} \cdot \nabla f$ and p the pressure. Applying the product rule $\mathrm{D}(\rho \mathbf{u})/\mathrm{D}t = (\mathrm{D}\rho/\mathrm{D}t)\mathbf{u} + \rho \mathrm{D}\mathbf{u}/\mathrm{D}t$ and using the continuity equation (26), conservation of mass may also be written on the compact but non–conservative form

$$\rho \frac{\mathrm{D}\mathbf{u}}{\mathrm{D}t} + \nabla p = \nabla \cdot \sigma \ .$$

The Cauchy stress tensor is given by

$$\sigma = \lambda (\nabla \cdot \mathbf{u}) I + \mu \left(\nabla \mathbf{u} + (\nabla \mathbf{u})^T \right) \ .$$

Assuming constant entropy, the system is closed by an equation of state $p = p(\rho)$, for example the gamma–law $p = \rho^\gamma$ with $\gamma = 1.4$ for air under normal conditions.

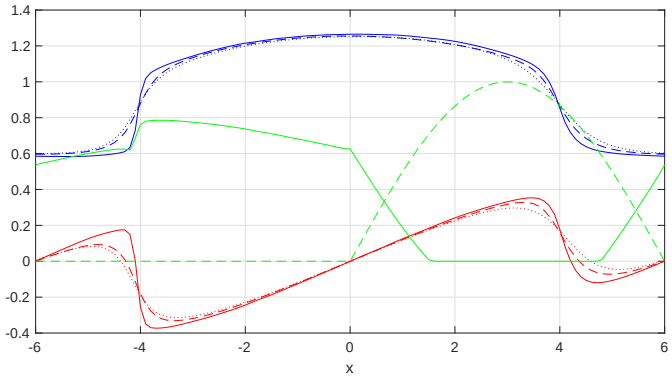

FIGURE 10. Approximations to Navier–Stokes system (27) at $t = 6$, $\Delta x = 0.1$, CFL=0.8 and 0.4 (hr). Density (blue), velocity (red), diffusion (green). Local Lax–Friedrichs (dotted), adaptive E (dashed), and hr adaptive E (solid).

In conservative form and in one space variable, the system reads

$$\begin{pmatrix} \rho \\ \rho u \end{pmatrix}_t + \begin{pmatrix} \rho u \\ \rho u^2 + p \end{pmatrix}_x = \begin{pmatrix} 0 \\ (\lambda + 2\mu) u_x \end{pmatrix}_x \quad . \tag{27}$$

Fig. 10 shows the adaptive E–scheme in comparison to local Lax–Friedrichs when applied to the one–dimensional system (27) with given diffusion

$$(\lambda + 2\mu)(x) = \max\left(0, \frac{1}{20} \sin\left(\frac{x\pi}{6}\right)\right) \quad .$$

Note that for negative $x < 0$ the system degenerates to the inviscid, isentropic Euler equations. The initial density is $\rho(0, x) = 1.0 - 0.5\cos(x\pi/6)$ with zero initial momentum and periodic boundary conditions. The mesh size Δx is 0.1 with CFL number 0.8 for local Lax–Friedrichs and adaptive E–schemes. The high–resolution adaptive E–scheme uses minmod slopes [19]. It lives on a five–point stencil and hence the CFL limit is 0.5. The CFL number for the simulations shown in Fig. 10 is 0.4.

On the right hand side we see a by natural diffusion smoothed out and right going wave. Here the adaptive E–scheme is sharper than classical Lax–Friedrichs due to less artificial diffusion. On the left hand side a shock–wave forms. Due to lack of natural diffusion, the adaptive E–scheme reduces to local Lax–Friedrichs. Especially in this regime the minmod limited slopes help to increase resolution.

Our last experiment simulates "dancing" waves in the two–dimensional Navier–Stokes system

$$\begin{pmatrix} \rho \\ \rho u \\ \rho v \end{pmatrix}_t + \begin{pmatrix} \rho u \\ \rho u^2 + p \\ \rho uv \end{pmatrix}_x + \begin{pmatrix} \rho v \\ \rho uv \\ \rho v^2 + p \end{pmatrix}_y = \begin{pmatrix} 0 \\ (\lambda + 2\mu) u_x + (\lambda + \mu) v_y \\ \mu v_x \end{pmatrix}_x + \begin{pmatrix} 0 \\ \mu u_y \\ (\lambda + \mu) u_x + (\lambda + 2\mu) v_y \end{pmatrix}_y \quad . \tag{28}$$

with degenerate, density–dependent dynamic viscosity

$$\mu(\rho, x) = \frac{\rho}{20} \max\left(0, \frac{3}{10} + \sin\left(\frac{x\pi}{6}\right) \sin\left(\frac{y\pi}{6}\right)\right)$$

and Stokes hypothesis $3\lambda + 2\mu = 0$. The initial density is a perturbed sin–wave

$$\rho(0, x, y) = 1 + \frac{1}{10} \sin\left(\frac{(x-6)\pi}{3}\right) \sin\left(\frac{(y+3)\pi}{3}\right)$$

with $\rho(0, x, y) = 0.25$ within the rectangle $[-3, 3] \times [-2, 2]$. At time $t = 0$ the flow is at rest, i.e. $(u, v) = (0, 0)$. The mesh is uniform and square with $\Delta x = \Delta y = 1/20$.

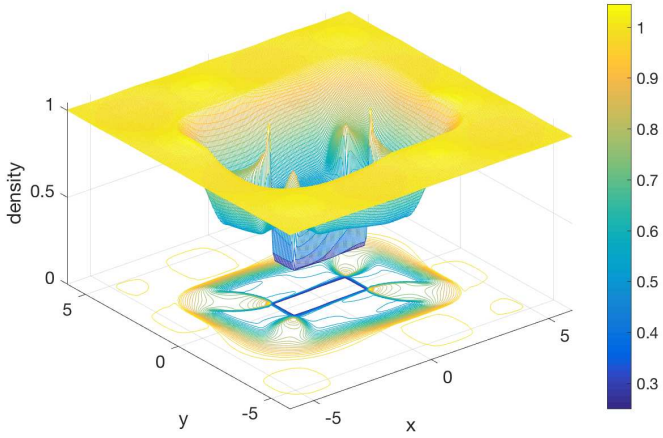

FIGURE 11. Density in 2d Navier–Stokes (28) at $t = 1$, $\Delta x = \Delta y = 1/20$, CFL=0.5.

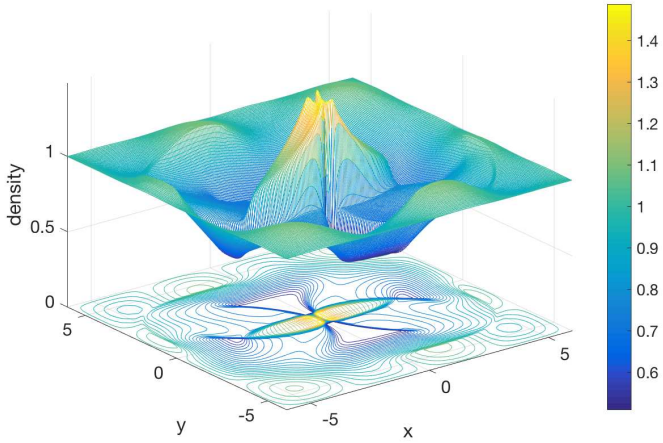

FIGURE 12. Density in 2d Navier–Stokes (28) at $t = 2$, $\Delta x = \Delta y = 1/20$, CFL=0.5.

Natural viscosities given in (28) are $d^x = (0, \lambda + 2\mu, \mu)^T$ and $d^y = (0, \mu, \lambda + 2\mu)^T$. Artificial viscosities are adapted component– and coordinatewise such that the total, effective viscosity $D = d + \epsilon\Delta x$ is nowhere less than the local characteristic speed in each direction $|u| + \sqrt{p'(\rho)}$ and $|v| + \sqrt{p'(\rho)}$ respectively. As there is no natural diffusion in the continuity equation, the numerical viscosity for ρ is strictly positive. This is in contrast to the momentum equations where numerical viscosities degenerate locally. The time step is limited by (20) applied coordinate– and component–wise, i.e. the maximum taken over all three components and in both directions to determine a global time step. The CFL number for the simulations shown here is 0.5. We apply the high–resolution, adaptive E–scheme with monotonized central limiter [19].

Despite low and degenerate artificial viscosities, the scheme is stable and produces approximations free of spurious oscillations as displayed in Figs. 11 and 12. In Fig. 13 we observe the ρ–dependent natural diffusion deceasing to zero on the left side. Like in the one–dimensional experiment above, the adaptive viscosity E–scheme develops its potential in the presence of natural diffusion as can bee seen around $x = 2$. The limited slopes in contrast increase resolution in the hyperbolic regime and especially around $x = -4$.

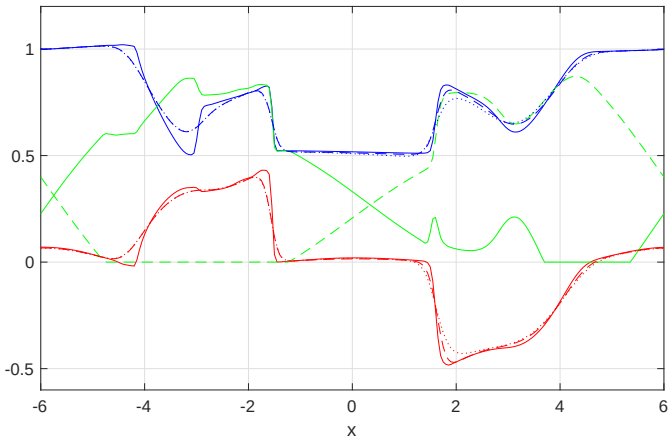

FIGURE 13. Cross–section along $y = 1$ at $t = 1$. Density ρ (blue), x–momentum ρu (red). Upscaled natural diffusion $(\lambda + 2\mu)/\Delta x$ (green dashed), artificial diffusion (green solid). Local Lax–Friedrichs (dotted), adaptive E (dashed), and hr adaptive E (solid).

Fig. 14 displays a considerable increase in resolution as compared to local Lax–Friedrichs at $t = 2$; actually the relative deviation is 40%. Also in comparison to hr local Lax–Friedrichs using mc–limited slopes, see Fig. 15, we still find a relative improvement of 8% which comes essentially for free. To adapt the numerical viscosity dynamically does not cost any extra computations. In contrast, the time–step actually may increase with less diffusion overall.

13. Stability when applied to balance laws

Consider

$$u_t + f(u)_x = (d(u, x)u_x)_x + g(u) \tag{29}$$

with

$$f, g \in C^1(\mathbb{R}) \ , \quad \|f'\|_\infty < \infty \ , \qquad \nu \le g' \le \mu \ , \quad d(u, x) \ge 0 \ .$$

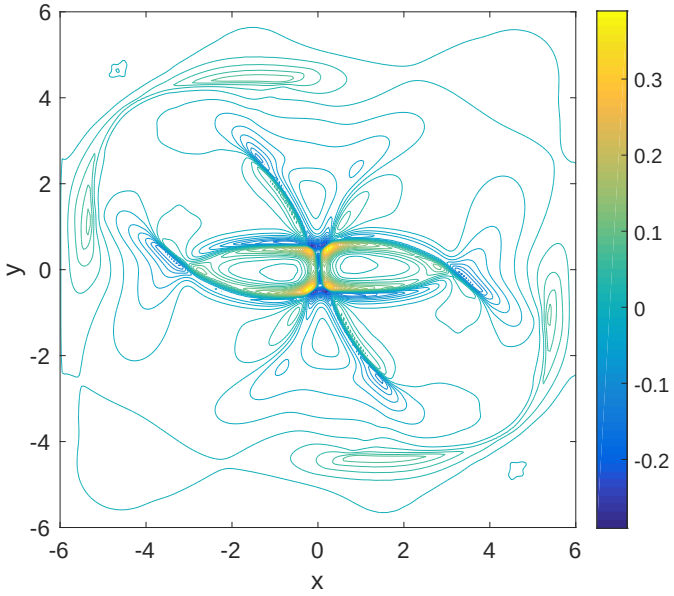

FIGURE 14. Difference in density between hr adaptive E and local Lax–Friedrichs at $t = 2$.

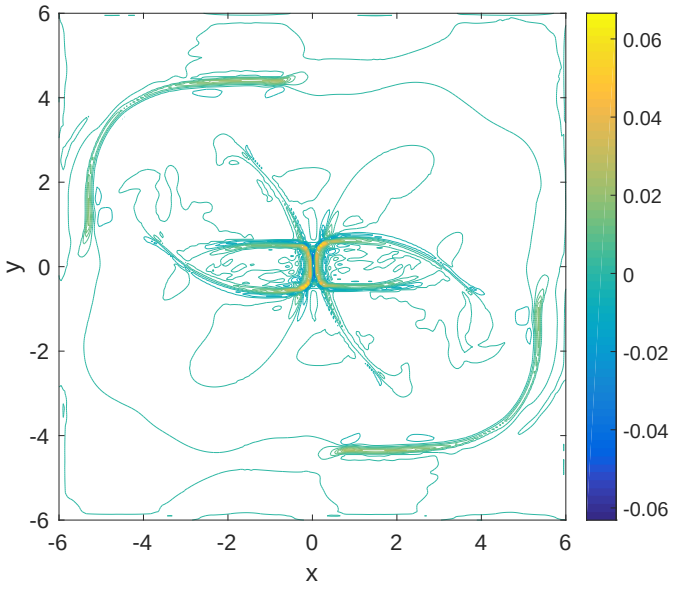

FIGURE 15. Difference in density between hr adaptive E and hr local Lax–Friedrichs both using mc–limited slopes, $t = 2$.

Three point E–schemes applied to balance laws are monotone. The following lemma generalizes Corrolary 5.3.

Lemma 13.1. *Let F be a consitent E–flux (9). Under the CFL–condition*

$$\frac{\Delta t}{\Delta x}\|F_v - F_w\|_\infty \leq 1 + \Delta t\nu \tag{30}$$

the augmented discrete operator

$$H(u_{j-1},u_j,u_{j+1}) = u_j - \frac{\Delta t}{\Delta x}\left(F(u_j,u_{j+1}) - F(u_{j-1},u_j)\right) + \Delta t g(u_j) \tag{31}$$

is monotone.

Proof. By Lemma 5.1 the flux is quasi–monotone. Thus

$$\partial_{u_{j-1}} H = \frac{\Delta t}{\Delta x}\partial_{u_{j-1}} F(u_{j-1},u_j) \geq 0$$

and

$$\partial_{u_{j+1}} H = -\frac{\Delta t}{\Delta x}\partial_{u_{j+1}} F(u_j,u_{j+1}) \geq 0 \ .$$

due to the assumption (30)

$$\partial_{u_j} H = 1 - \frac{\Delta t}{\Delta x}\left(\partial_{u_j} F(u_j,u_{j+1}) - \partial_{u_j} F(u_{j-1},u_j)\right) + \Delta t g'(u_j) \geq 0 \ .$$

This completes the proof. □

Moreover, ϑ–time stepping for the operator (31)

$$\frac{1}{\Delta t}(u^{n+1}-u^n) = \vartheta\left(F_{\Delta x}+G\right)(u^{n+1}) + (1-\vartheta)\left(F_{\Delta x}+G\right)(u^n) \tag{32}$$

with $0 \leq \vartheta \leq 1$, conservative space discretization (13) and the diagonal field $G(u)_j = g(u_j)$ is stable in the sense of Hadamard. To this end consider the scheme expressed as an operator root equation

$$T_h = \begin{pmatrix} u^0 - u(0,\cdot) \\ L_h(u^n) - R_h(u^{n-1}) \ , \quad n = 1,2,\ldots,N \end{pmatrix} = 0 \tag{33}$$

with the augmented left– and right–hand sides

$$L_h(v) = \frac{1}{\Delta t}v - \vartheta\left(F_{\Delta x}+G\right)(v) \ , \quad R_h(v) = \frac{1}{\Delta t}v + (1-\vartheta)\left(F_{\Delta x}+G\right)(v) \ .$$

The discrete solution operator, that is the numerical scheme, is given by the inverse operator $\widehat{u} = T_h^{-1}(0)$. Stability means that T_h^{-1} is uniformly Lipschitz continuous

$$\|u-v\| \leq S\|T_h(u) - T_h(v)\| \ , \tag{34}$$

with a stability constant S independent of $h = (\Delta t, \Delta x)$. Taking $\widetilde{u}$ as the solution to the balance law (29), convergence follows, assuming the method is consistent in the sense

$$\|\widetilde{u}|_h - \widehat{u}\| \leq S\|T_h(\widetilde{u}|_h)\| \to 0 \ , \quad h \to 0 \ .$$

Lemma 13.2. *Under the time step restrictions*

$$\vartheta\mu\Delta t \leq \kappa < 1 \ , \quad (1-\vartheta)\left(\frac{\Delta t}{\Delta x}\|\partial_v F - \partial_w F\|_\infty - \Delta t\frac{\nu+\mu}{2}\right) \leq 1 \ ,$$

the ϑ–scheme (33) with conservative $F_{\Delta x}$ (13) and consistent E–flux (9) is stable i.e. there is a stability constant such that (34) holds.

Proof. To verify the stability inequality (34) it is natural to consider

$$T_h^n(u) - T_h^n(v) = L_h(u^n) - L_h(v^n) - \left(R_h(u^{n-1}) - R_h(v^{n-1})\right) \ , \quad n = 1,2,\ldots,N.$$

By the mean value theorem

$$A_h^n(u^n - v^n) = T_h^n(u) - T_h^n(v) + B_h^{n-1}(u^{n-1} - v^{n-1}) \tag{35}$$

with

$$A_h^n = \frac{1}{\Delta t} I - \vartheta \int_0^1 D\left(F_{\Delta x} + G\right)(\xi(s))\, \mathrm{d}s \ ,$$

$$B_h^n = \frac{1}{\Delta t} I + (1-\vartheta) \int_0^1 D\left(F_{\Delta x} + G\right)(\xi(s))\, \mathrm{d}s \ , \quad \xi(s) = v^n + s(u^n - v^n) \ .$$

By Lemma 5.1, the consistent E–flux is quasi–monotone and $DF_{\Delta x}$ is quasi–positive. The additional diagonal field G does not effect quasi–positivity of the augmented Jacobian $D\left(F_{\Delta x} + G\right) = DF_{\Delta x} + \mathrm{diag}(g'(u_j))$. Due to the conservation form (13) $DF_{\Delta x}^T \delta \leq 0$. By the Lipschitz–bound for g' it holds $D\left(F_{\Delta x} + G\right)^T \delta \leq \mu\delta$ and thus

$$(A_h^n)^T \delta \geq \left(\frac{1}{\Delta t} - \vartheta\mu\right) \delta \ .$$

Under the restriction $\Delta t \vartheta \mu \leq \kappa < 1$, A_h^n is M–matrix and

$$\|(A_h^n)^{-1}\|_1 = \|(A_h^n)^{-1}\delta\|_\infty \leq \frac{1}{\frac{1}{\Delta t} - \vartheta\mu} \leq \frac{\Delta t}{1-\kappa} = \mathcal{O}(\Delta t). \tag{36}$$

With $DF_{\Delta x}$ also B_h^n is quasi–positive. Unless the time step is restricted by (30) B_h^n cannot be expected to be monotone. Under the milder condition

$$(1-\vartheta)\left((DF_{\Delta x})_{jj} - \frac{\nu+\mu}{2}\right)\Delta t \leq 1 \ .$$

B_h^n is bounded

$$-P_h^n \leq B_h^n \leq P_h^n = \frac{1}{\Delta t} I + (1-\vartheta)\left(\int_0^1 DF_{\Delta x}(\xi(s))\, \mathrm{d}s + \mu I\right)$$

and $P_h^n \geq |B_h^n| \geq 0$ is monotone. Moreover, $(P_h^n)^T\delta \leq \frac{1}{\Delta t}\delta + (1-\vartheta)\mu\delta$. Thus,

$$\|P^n\|_1 = \|(P^n)^T\|_\infty = \|(P^n)^T\delta\|_\infty \leq \frac{1}{\Delta t} + (1-\vartheta)\mu \ .$$

In combination with (36)

$$\|(A^n)^{-1}P^{n-1}\|_1 \leq \frac{\Delta t}{1-\vartheta\mu\Delta t}\left(\frac{1}{\Delta t} + (1-\vartheta)\mu\right) \leq 1 + \frac{\max(\mu,0)}{1-\kappa}\Delta t \ . \tag{37}$$

From (35) with (36) and (37) it follows

$$\|u^n - v^n\|_1 = \mathcal{O}(\Delta t)\|T_h^n(u) - T_h^n(v)\|_1 + (1+\mathcal{O}(\Delta t))\|u^{n-1} - v^{n-1}\|_1 \ .$$

With a suitable constant and by iteration, find

$$\begin{aligned}
&\|u^n - v^n\|_1 \\
&\leq (1+c\Delta t)^n \, \|T_h^0(u) - T_h^0(v)\|_1 + \sum_{l=1}^{n} (1+c\Delta t)^{n-1}\, c\Delta t \|T_h^l(u) - T_h^l(v)\|_1 \\
&\leq e^{cn\Delta t}\,(1+cn\Delta t) \max_{l=0,\ldots,n} \|T_h^l(u) - T_h^l(v)\|_1 \ , \quad \forall n\Delta t \leq T \ .
\end{aligned}$$

Finally, stability follows $\|u-v\|_{1,\infty} \leq (1+cT)\, e^{cT} \|T_h(u) - T_h(v)\|_{1,\infty}$. □

14. Conclusions

The three–point, adaptive viscosity E–scheme is monotone and TVD. It reduces numerical diffusion whenever there is enough natural (given) diffusion. Without numerical diffusion, the scheme is second order accurate. In the convection dominated case, the scheme adaptively turns on artificial viscosity and reduces to first order. By construction it cannot resolve diffusive effects below the stability threshold. Nevertheless, high resolution is achieved by the application of TVD limited slopes and/or mesh refinement. The high–resolution adaptive E–scheme is not necessarily monotone, thus not limited to first order, but TVD. The method is stable and accurate independent of natural viscosity. Hence, it applies to fully nonlinear and degenerate viscous conservations laws. With fully implicit time stepping the scheme is unconditionally stable and therefore well–suited for adaptive mesh refinement to resolve shock positions and low diffusion effects. An adaptive, discontinuous Galerkin E–scheme on multidimensional domains is currently under development.

Acknowledgments

This research was supported by the Ethiopian Department of Education and the Norwegian Agency for Development Cooperation.

References

[1] Bohl, E. *Finite Modelle gewhnlicher Randwertaufgaben*. Teubner, Stuttgart, 1981.
[2] Breuss, M. The implicit upwind method for 1-D scalar conservation laws with continuous fluxes. *SIAM J. Numer. Anal. 43*, 3 (2005), 970–986.
[3] Breuss, M. Monotonicity of implicit finite diffeence methods for hyperbolic conservation laws. *Preprint*, 253 (2009).
[4] Chen, G.-Q., and Karlsen, K. H. L^1-framework for continuous dependence and error estimates for quasilinear anisotropic degenerate parabolic equations. *Trans. Am. Math. Soc. 358*, 3 (2006), 937–963.
[5] Crandall, M. G., and Majda, A. Monotone difference approximations for scalar conservation laws. *Math. Comput. 34*, 149 (1980), 1–21.
[6] Evje, S., and Karlsen, K. H. Discrete approximations of BV solutions to doubly nonlinear degenerate parabolic equations. *Numer. Math. 86*, 3 (2000), 377–417.
[7] Evje, S., and Karlsen, K. H. Monotone difference approximations of BV solutions to degenerate convection-diffusion equations. *SIAM J. Numer. Anal. 37*, 6 (2000), 1838–1860.
[8] Fiedler, M., and Pták, V. On matrices with non–positive off–diagonal elements and positive principal minors. *Czech. Math. J. 43* (1962), 382–400.
[9] Gustafsson, B., Kreiss, H.-O., and Sundström, A. Stability theory of difference approximations for mixed initial boundary value problems II. *Math. Comput. 26*, 119 (1972), 649–689.
[10] Harten, A. High resolution schemes for hyperbolic conservation laws. *J. Comp. Math. Phys. 49* (1983), 357–393.
[11] Jin, S., and Xin, Z. The relaxation schemes for systems of conservation laws in arbitrary space dimensions. *Comm. Pure Appl. Math. 48* (1995), 235–276.
[12] Karlsen, K. H., Koley, U., and Risebro, N. H. An error estimate for the finite difference approximation to degenerate convection-diffusion equations. *Numer. Math. 121*, 2 (2012), 367–395.
[13] Karlsen, K. H., Risebro, N. H., and Storrøsten, E. B. L^1 error estimates for difference approximations of degenerate convection-diffusion equations. *Math. Comput. 83*, 290 (2014), 2717–2762.
[14] Karlsen, K. H., Risebro, N. H., and Storrøsten, E. B. On the convergence rate of finite difference methods for degenerate convection-diffusion equations in several space dimensions. *ESAIM, Math. Model. Numer. Anal. 50*, 2 (2016), 499–539.
[15] Koren, B. A robust upwind discretization method for advection, diffusion and source terms. In *Numerical methods for advection-diffusion problems*. Braunschweig: Vieweg, 1993, pp. 117–138.
[16] Kreiss, H.-O. Initial boundary value problems for hyperbolic partial differential equations. *Proc. ICM Vancouver* (1974), 127–137.
[17] Kreiss, H. O., and Lorenz, J. *Initial–Boundary Value Problems and the Navier–Stokes Equations*. Academic Press, Bosten, 1989.
[18] Kröner, D. *Numerical Schemes for Conservation Laws*. Wiley, Teubner, Stuttgart, 1997.

[19] LeVeque, R. *Finite Volume Methods for Hyperbolic Problems*. Cambridge Univ. Press, 2002.
[20] Natalini, R. Convergence to equilibrium for the relaxation approximations of conservation laws. *Comm. Pure Appl. Math. 49* (1996), 795–823.
[21] Osher, S. Riemann solvers, the entropy condition, and difference approximations. *SIAM J. Numer. Anal. 21* (1984), 217–235.
[22] Rusanov, V. The calculation of the interaction of non-stationary shock waves and obstacles. *USSR Computational Mathematics and Mathematical Physics 1*, 2 (1962), 304 – 320.
[23] Schroll, H. J. High-resolution relaxed upwind schemes in gas dynamics. *J. Sci. Comput. 17*, 1-4 (2002), 599–607.
[24] Schroll, H. J. Relaxed high-resolution schemes for hyperbolic conservation laws. *J. Sci. Comput. 21*, 2 (2004), 251–279.
[25] Tadmor, E. Numerical viscosity and the entropy condition for conservative difference schemes. *Math. Comput. 43* (1984), 369–381.

Department of Mathematics and Statistics, Hawassa University, Hawassa, Ethiopia
E-mail: ebiatye2020@gmail.com

Department of Mathematics and Computer Science, University of Southern Denmark, Odense
E-mail: achim@imada.sdu.dk